Cellular and Network Mechanisms of Grid Cell Firing Patterns

A thesis submitted in partial fulfillment of the requirements of IISER Pune's BS-MS dual degree programme.

Submitted by

Sahana V Srivathsa

Reg no: 20121024

Indian Institute of Science Education and Research, Pune

Thesis advisor:

Dr. Collins Assisi

Indian Institute of Science Education and Research, Pune

Certificate

This is to certify that this dissertation entitled "*Cellular and Network Mechanisms of Grid Cell Firing Patterns*" towards the partial fulfillment of the BS-MS dual degree programme at the Indian Institute of Science Education and Research (IISER), Pune represents original research carried out by Sahana V Srivathsa at IISER Pune under the supervision of Dr. Collins Assisi, Assistant Professor, Biology Division, IISER Pune during the academic year 2016-2017.

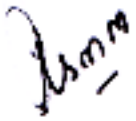

30/03/17

Dr. Collins Assisi

Date

Declaration

I hereby declare that the matter embodied in the report entitled "*Cellular and Network Mechanisms of Grid Cell Firing Patterns*" are the results of the work carried out by me at the Department of Biology, Indian Institute of Science Education and Research (IISER), Pune, under the supervision of Dr. Colins Assisi, IISER Pune, and the same has not been submitted elsewhere for any other degree.

Sahana Srivathsa

Sahana V. Srivathsa

30/03/2017

Date

Abstract

Grid cells in the entorhinal cortex encode information about spatial representation by firing at hexagonally spaced intervals that tile the local environment. Stellate cells (SCs) are thought to be putative grid cells and our aim is to understand how the intrinsic cellular properties of SCs affect the firing fields of grid cell networks. We aimed to achieve this by recreating a detailed mathematical model of a SC (based on previous experimentally constrained models) and study how key conductances in this model characterize its dynamics and the role of these intrinsic properties at a network level. The distinct features of stellate cells we studied using simulations were the generation of subthreshold oscillations and clustering of action potentials. By building simplistic networks of excitatory SCs and inhibitory interneurons, we were able to show how changes in synaptic input to SCs via variations in inhibitory inputs affected the clustering of SCs. Understanding mechanisms governing the cellular and network level properties can help provide insights into the factors governing grid cell firing fields and spatial representation.

Table of Contents

List of Figures

Acknowledgments

I would like to thank Dr. Collins Assisi for his all his support, encouragement and advice during the course of my project. It was an educational and enjoyable experience working. I would also like to thank the members of my lab for their insightful inputs, lively conversation and numerous cups of fortifying tea that proved invaluable. The support of my family and friends during this year was immeasurably comforting and I thank them as well. Finally, I would like to extend my gratitude towards IISER Pune, for providing me with this opportunity and the chance to learn and grow over these five truly memorable years.

1. Introduction

1.1 Neural Representation of Space

Animals' ability to navigate through their surrounding environment, is attributed to the neural encoding of their spatial orientation and information about their surroundings. Spatial memory and the concept of neural representation of space through the encoding and decoding of attributes of the spatial environment termed as a cognitive map, was first proposed by Tolman in 1984, who demonstrated the ability of rats to navigate mazes by remembering cues (Tolman, 1948). The hippocampus was the first region of the brain to be associated with spatial representation with the discovery of place cells. Place cells, thought to be the pyramidal neurons in the CA regions hippocampus, fire when the animal is at a certain location in the environment (O'Keefe & Dostrovsky, 1971; O'Keefe, 1976). Adjacent place cells fire when the animal is positioned at adjacent locations, thus creating a map of the entire local environment (O'Keefe, 1976; Wilson & McNaughton, 1993). Providing dynamic representations of space the relative position of the firing fields varies, while the same place cells may be used in different environments (Nadel, 1991; John O'Keefe & Conway, 1978). Apart from spatial navigation, these neurons are also associated with storing and retrieving declarative and episodic memory encoded as temporal sequences of spikes (Eichenbaum, et al., 1999) though the spatial and non-spatial variables are independently represented, the former through firing location and the latter via firing rate (Hampson, et al., 1993; Leutgeb et al., 2005).

Firing in place cells is determined by two independent types of inputs: external stimuli from the environment and self positioning by integration of linear and angular self motion known as path integration(Etienne & Jeffery, 2004; Pastalkova et al., 2008; Quirk et al., 1990). It has been shown that place cells receive inputs from neurons in

various layers of the entorhinal cortex (EC) which also exhibit correlated patterns of spatial firing, indicating that location signals involve computations outside the hippocampus (Brun et al., 2002; Samsonovich & McNaughton, 1997). Neurons in the II and III layers of the medial entorhinal cortex (MEC), termed as grid cells, project into the CA1 of the hippocampus have multiple firing fields (Fyhn, et al., 2004). These grid cells fire when the animal is at the vertices of a hexagonally symmetric grid that tiles the entire local environment of the animal (Hafting, et al., 2005).

Unlike sensory neurons encoding a single sensory modality, these MEC neurons receive convergent polymodal inputs from the neocortex that help in determining the animal's position with respect to its environment (Moser, et al., 2008). As the phase and orientation of neighboring grid cells remains conserved across different environments (McNaughton, et al., 2006; Sargolini et al., 2006), the path integration input to the place cells is thought to be provided by computations in the grid cells that in turn use inputs from head direction and speed cells to dynamically determine self position(Kropff, et al., 2015). Several theoretical models have been proposed to explain the emergence of grid cell firing properties at a cellular and network level (Zilli, 2012), however, there is a dearth of recordings from single neurons in the MEC leaving us unable to definitively determine the exact mechanisms of how synaptic inputs at the level of a single neuron are converted into grid cell firing (Schmidt-Hieber & Häusser, 2013).

1.2 Characterization of Stellate Cells

The MEC has two types of excitatory projection neurons, namely, stellate cells and pyramidal cells and three intermediate cell types (Canto & Witter, 2012). Stellate cells are the primary excitatory neuron present in the II layer of the MEC (Sargolini et al., 2006), a region with the majority of grid cells and possess firing fields indicative of grid like firing patterns. Therefore, we can consider stellate cells, henceforth referred to as SCs, to be putative grid cells (Schmidt-Hieber & Häusser, 2013). Through

path-clamp and EEG recordings, the distinct intrinsic physiological properties of SCs have been identified, however it is still not yet known how these properties play a role in determining the firing patterns of grid cells. SCs are morphologically characterized by the distinct stellar architecture of their dendrites which are longer and have more complex morphology than non stellate cells. They usually have one or two thicker, primary dendrites and the axons, nearly double the thickness of non SCs, emerge from near the primary dendrite (Klink & Alonso, 1997).

The membrane potential of SCs produces subthreshold oscillations with a frequency in the theta range (4-12 Hz) when depolarized to close to the threshold for generating action potentials (Alonso & Klink, 1993; Dickson, et al., 2000). Theta frequency oscillations are considered a potential candidate to encode spatial information in the grid cells, based on observations of network level theta rhythms in the hippocampus and MEC. (Burgess, et al., 2007; Dickson, et al., 2000) Though the cells in the same region of the MEC have similar grid orientation, the spatial frequency of the grid like firing fields increases monotonically from the dorso-medial to ventro-lateral regions of the MEC (Hafting et al., 2005; Sargolini et al., 2006) which mirrors the increase in place fields along the dorsoventral axis of the hippocampus (Canto & Witter, 2012). The intrinsic properties of SCs in terms of subthreshold oscillations and resonance activity as well as integration of synaptic responses also show a concomitant variation along the MEC and could thus potentially offer insights into cellular mechanisms affecting spatial representation (Garden, et al., 2008; Giocomo, et al., 2007).

In SCs, the subthreshold oscillations are thought to be generated by the interactions between a persistent sodium current (I_{NaP}) and a non-specific hyperpolarization activated inward current (I_h) (Dickson, et al., 2000, Magistretti,& Alonso, 1999). The h-current also causes a characteristic depolarizing “sag” in the membrane potential when hyperpolarized (McCormick & Huguenard, 1992). Other characteristic properties of SCs such as clustering of action potentials and mixed-mode oscillations in membrane voltage, an alternation between subthreshold oscillations and action

potential spikes, are caused by interactions between the h-current and other potassium currents (Fransén, et al., 2004). In this project, we aimed to recreate a detailed mathematical model of a stellate cell (based on an experimentally constrained model by (Fransén, et al., 2004) in order to study the effect of the intrinsic properties of SCs at a network level.

Excitatory SCs are connected to each other via inhibitory interneurons, the intermediate cell types mentioned earlier. Intracellular recordings from these neurons show that they are powerful fast-spiking neurons mediated by NMDA receptors (Jones & Bühl, 1993). Computational models of grid cells are based on competition between long range inhibition and short range activation to produce hexagonal patterns. These models propose two mechanisms of inhibitory activity: The classical interneurons that hyperpolarize the membrane potential of SCs and the second is individual properties of the neuron such as spike time dependent plasticity which cause the neuron to stop firing (Rowland, et al., 2016). In the interneurons of the entorhinal cortex, modeling spike timing dependent plasticity (STDP), shown to be dependent on intracellular calcium levels from experimental data, suggests that modulating the strength of a few interneurons can modulate an entire network of excitatory SCs (Haas, et al., 2006). By simulating simple networks of SCs and interneurons, we aim to understand how the proposed inhibitory mechanisms of grid cells affect the synaptic output of realistic representations of SC networks. This will hopefully provide insights into the role of intrinsic properties of SCs in defining the attributes of grid cell firing fields and its modification with learning.

2. Materials and Methods

All biophysical simulations were run using *insilico,* a C++ library of classes that can be used to integrate differential equations to describe the conductance-based ion channels in neurons and thus study neuronal activity. The current dynamics were modeled according to Hodgkin-Huxley equations.(Hodgkin & Huxley, 1990) All units used in the simulation conform to the default units used in NEURON unless specified otherwise. These simulations primarily rely on voltage clamp data to analyze how the interactions between currents leads to the characteristic behaviour of SCs as mentioned above.

2.1 The Stellate Cell Model

The SC model was based on the seven compartmental model proposed by Fransen with parameters modified to fit experimental data (Fransén et al., 2004). As SCs span multiple layers of the EC multi-compartmental models provide a more physiologically accurate model as they incorporating attenuation of signals. A schematic representation of cylindrical compartments along with their dimensions is detailed in the figure below.

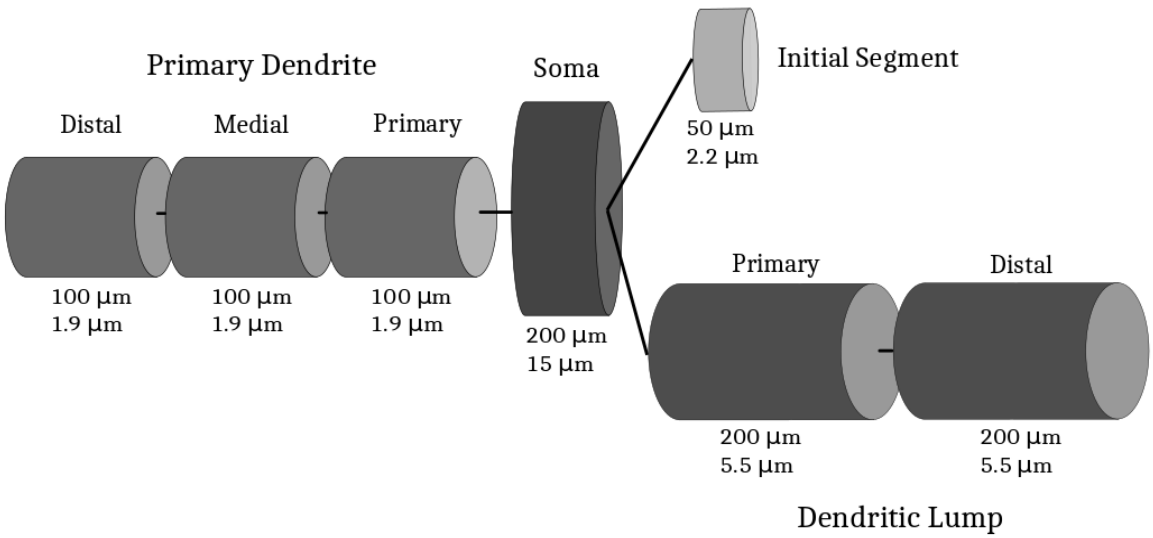

Fig 1: Schematic Representation of SC multi-compartmental model

The central singular compartment, the soma, is connected to three different compartments: initial segment (axon) represented by a single compartment, a single primary dendrite divided into three identical compartments connected in succession and the main load to the soma provided by a “lump” or group of the remaining dendrites represented by two identical compartments. The attenuation of synaptic inputs to cells is accurately represented by the multiple dendritic compartments.

The length and diameters were adjusted to comply with the sealed end boundary condition. The passive parameters represent the initial conditions of the neuron and are used to calculate the resistive coupling between adjacent compartments. The values of the resting membrane potential(E_m), the input resistance (R_m) and capacitance (C_m) are as follows:

E_m = - 83 mV, R_m = 100 Ωcm, C_m = 1μcm

The resistive coupling between compartments is calculated according to the following formula. (Sterratt,et al., 2011)

$$\mathrm{g}_{i,i+1} = \left(\frac{(d_{i+1}+d_i)^2}{16 d_i \; R_a \; l^2}\right) \left(\mathrm{v}_{i+1} - v_i\right)$$

where,

$g_{i,i+1)}$ = resistive coupling from compartment i+1 to I, i = compartment index, d_i = diameter of compartment, R_a = input resistance, v_i = membrane potential of compartment, l = length of compartment I.

The membrane potential E_m depends only on the Na^+ and Cl^- leaks, as the K^+ leakage is represented as a separate current. In order to mimic the conductance based noise source included in the current clamp simulations, (White, et al., 1998) a noise term was included in the simulations and added to the proximal lumped dendritic compartment. The noise was generated through the C++ internal Poisson process with a mean of 200Hz, reversal potential of 45mV, conductance of 9.4 pS and time constant of 3 ms.

2.1.1 A Minimal Model

In order to understand the role of individual currents in the dynamics of SCs, a simplified version of the model was first constructed containing only the hyperpolarization activated nonspecific cation current (I_h), a persistent low-threshold sodium current (I_{Nap}) and the potassium dependent leak current, to study the characteristic sub-threshold oscillations of SCs.

$$I_{ion} = I_h + I_{NaP} + I_{K(leak)} \qquad \text{(Equation 1)}$$

The dynamics of the currents were represented using HH equations. The I_h current is described by two independent components: a fast and a slow one which interact with each other and the persistent sodium to produce sub-threshold oscillations. The slow and fast components are based on experimental data from (Dickson, Magistretti, Shalinsky, Fransén, et al., 2000) and the biexponential curve fitting to describe the currents in (Fransén et al., 2004).The parameters for the steady state activation and inactivation kinetics of I_{Nap} was modeled based on experimental evidence from (Magistretti & Alonso, 1999; Magistretti et al., 1999). The reversal potential and exponents of the activation rates were based on (Huguenard & McCormick, 1992). The conductance for the IS compartment is 0.0mS/cm^2 for all currents except the leak. The following equations represent the parameters for the H-H equations of the two currents.

NaP Current: (E_{rev} = + 87mV)

Conductance of all compartments except IS: $g_{NaP} = 0.038 mS/cm^2$

Activation: (x)

$$\mathrm{x}_{inf}(V) = \frac{1.0}{1 + exp(-\frac{(V+48.7)}{4.4})}$$

$$\frac{1}{\tau_x(V)} = \frac{0.091 * (V+38)}{1 - exp(-\frac{(V+38)}{5})} + \frac{-0.062 * (V+38)}{1 - exp(-\frac{(V+38)}{5}}$$

$$\text{Gate exponent} = 1$$

Inactivation: (y)

$$\alpha_y(V) = \frac{(-.00288\ V) - 0.049}{1 - exp(-\frac{(V + (0.049)/(0.00288)}{4.63})}$$

$$\beta_y(V) = \frac{(0.00694\ V) + 0.447}{1 - exp(-\frac{(V + (0.447)/(0.00694)}{-2.63})}$$

$$\tau_y(V) = \frac{1}{(\alpha_h + \beta_h)} \quad , \quad \mathrm{y}_{inf}(V) = \frac{\alpha_h}{(\alpha_h + \beta_h)}$$

$$\text{Gate exponent} = 1$$

h - Current: (E_{rev} = - 20mV)

Fast: (h_f)

Conductance of all compartments except IS: $g_{hf} = 0.098 mS/cm^2$

$$\tau_{hf}(V) = \frac{0.51}{exp\ \frac{V-1.7}{10} + exp - \frac{V+340}{52}\}}$$

$$\mathrm{m}_{inf(f)}(V) = \frac{1}{(1 + exp\ \frac{V+72.4}{9.78})^{1.36}}$$

Slow: (h_s)

Conductance of all compartments except IS: $g_{hs} = 0.053 mS/cm^2$

$$\tau_{hs}(V) = \frac{5.6}{exp\ \frac{V-17}{14} + exp - \frac{V+260}{43}\}}$$

$$\mathrm{m}_{inf(s)}(V) = \frac{1}{(1 + exp\ \frac{V+2.83}{15.9})^{58.8}}$$

$$\text{Gate exponent} = 1$$

K Leak Current: (E_{rev} = - 83mV) ,

Conductance of all compartments: $g_K = 0.058 mS/cm^2$

The Euler exponential method was employed to solve the differential equations and a time step of 5μs was used for all simulations. To observe the membrane potential "sag" effects of the SC, a hyperpolarizing current step of -0.06nA was simulated as

an external DC current injected into the soma. The duration of the pulse was varied but did not affect the sag effect observed.

2.1.2 The Detailed Model

To study the spike clustering behaviour of SCs as well as its mixed mode oscillations, a more detailed model including all the major currents was simulated.

$$\mathrm{I}_{ion} = I_{h(f)} + I_{h(s)} + I_{NaP} + I_{Na} + I_{K_{dr}} + I_{Ca_L} + I_{K_C} + I_{K(leak)}$$

(Equation 2)

The I_{Na} and I_{Kdr} (the delayed rectifier current) are responsible for the generation of spikes. I_{CaL} is a high threshold calcium current and I_{Kc} is a fast calcium and voltage dependent K^+ current which affects the clustering of spikes. The activation and inactivation variables and gate exponents for Na^+, K^+, Ca^{2+} currents were based on a model of hippocampal pyramidal cells.(Traub,et al., 1994; Traub, et al., 1991). The reversal potentials were based on (Fransén et al., 2004) and the conductances were adjusted to fit experimental data from (Alonso & Klink, 1993). See Appendix 1 for conductances for each compartment. The following equations represent the parameters for the activation and inactivation variables for the HH type equations of the other currents.

Na Current: (E_{rev} = + 87mV)

$$\mathrm{V'} = \mathrm{V} + 65$$

Activation: (m)

$$\alpha_m(V) = \frac{0.32\ (13.1 - V')}{exp(\frac{(13.1 - V')}{4}) - 1}$$

$$\beta_m(V) \frac{0.28\ (V' - 40.1)}{exp(\frac{(V' - 40.1)}{5}) - 1}$$

Gate exponent = 3

Inactivation: (h)

$$\alpha_h(V) = 0.128 \ * \ exp(\frac{(17-V')}{18})$$

$$\beta_h(V) = \frac{4}{exp(\frac{(40-V')}{5}) \ + \ 1}$$

Gate exponent = 1

$$\tau_y(V) = \frac{1}{(\alpha_h+\beta_h)} \quad , \quad \mathrm{y}_{inf}(V) = \frac{\alpha_h}{(\alpha_h+\beta_h)}$$

Kdr Current: (E_{rev} = - 83mV)

Activation: (n)

$$\alpha_n(V) = \frac{0.016 \ (35.1-V')}{exp(\frac{(35.1-V')}{5}) \ - \ 1}$$

$$\beta_n(V) = \frac{0.25}{exp(\frac{(20-V')}{40})}$$

Gate exponent = 4

CaL Current: (E_{rev} = + 80mV)

Activation: (s)

$$\beta_s(V) = \frac{0.02(V-51.1)}{exp(\frac{(V-51.1)}{5}) \ - \ 1}$$

$$\alpha_s(V) = \frac{1.6}{exp(-0.072(V-65)) \ + \ 1}$$

$$\text{Gate exponent} = 2$$

Kc Current: (E_{rev} = - 83 mV)

Activation: (c)

$$\text{If V} \leqslant 50mV:$$

$$\alpha_c(V) = \frac{(\frac{V'-10}{11}) - (\frac{V'-6.5}{27})}{18.975}, \qquad \beta_c(V) = \frac{0.02(V'-51.1)}{exp\frac{V-51.1}{5} - 1}$$

else:

$$\alpha_c(V) = 2exp(-\frac{V'-6.5}{27}), \qquad \beta_c = 0$$

$$\text{Gate exponent} = 1$$

2.2 Network Schematics

Stellate cells are excitatory cells connected via inhibitory interneurons. The inhibitory interneurons are modeled based on the single compartmental hippocampal interneurons simulated (Wang and Buzsáki, 1996) using Na^+ and K^+ currents also represented by HH equations. See appendix 2 for the parameters of the current dynamics. Both the inhibitory and excitatory connections between the neurons were modeled identically as tan-hyperbolic synapses with a reversal of the sign (positive or negative).

To study the effect of varying inhibitory inputs in a SC network, we considered 3 different network structures as depicted schematically below.

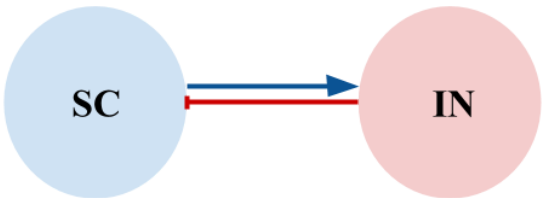

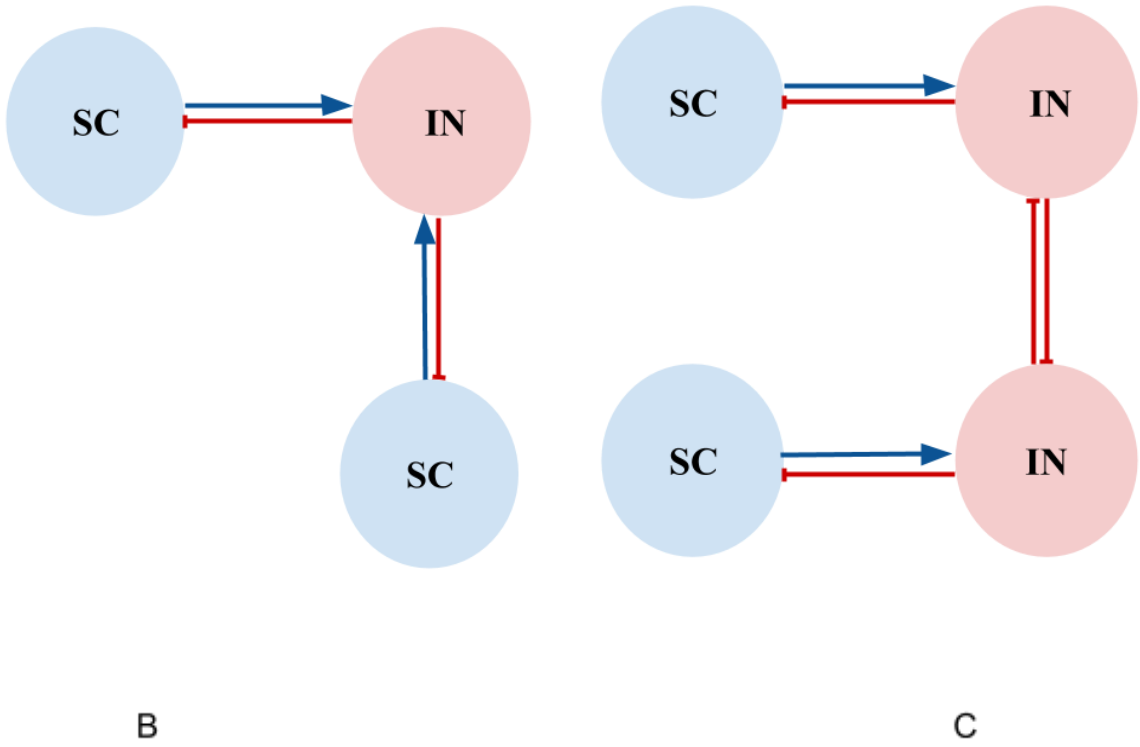

Fig 2: Schematic Representation of SC Networks

The blue cells represent the excitatory Stellate Cells and the red represents the inhibitory interneurons. The blue arrows are indicative of excitatory synaptic input while the red depict inhibitory connections in the three network motifs A, B and C.

On increasing the strength of inhibitory synapses projecting onto the SCs, by varying its conductances, we were able to gradually hyperpolarize the membrane potential of the SCs and observe the change in action potential firing.

3. Results and Discussion

Using the model described above, we were able to reproduce the characteristic features of stellate cells, in accordance with experimental data through which we were able to understand the factors influencing them, their interactions and the effect at a network level.

3.1 Intrinsic Properties of Stellate Cells

As the frequency and amplitude of subthreshold oscillations varies across the dorsoventral gradient (Giocomo et al., 2007; Pastoll, et al., 2012), understanding the currents that play a key role in their generation, allows us to identify potential new substrates of spatial representation.

In the minimal model of the stellate cell, we included only the I_h and I_{NaP} currents in order to observe their role in the generation of subthreshold oscillations. However, these oscillations could only be observed by depolarizing of the membrane potential in the range of the threshold of action potential firing (Fig 3) These oscillations are produced even in the absence of the noise coefficient, however the range over which oscillations are produced diminishes.

On individually plotting these currents, we can see they change during the oscillations. (Fig 4) The I_h current is an additive sum of independent slow and fast currents and its interplay with I_{NaP} is essential for the generation of these oscillations. The hyperpolarization activated I_h current increases in correlation with the membrane potential which in turn causes an increase in I_{NaP} which leads to a slight depolarization. The inward rectifying I_h current decreases on depolarization

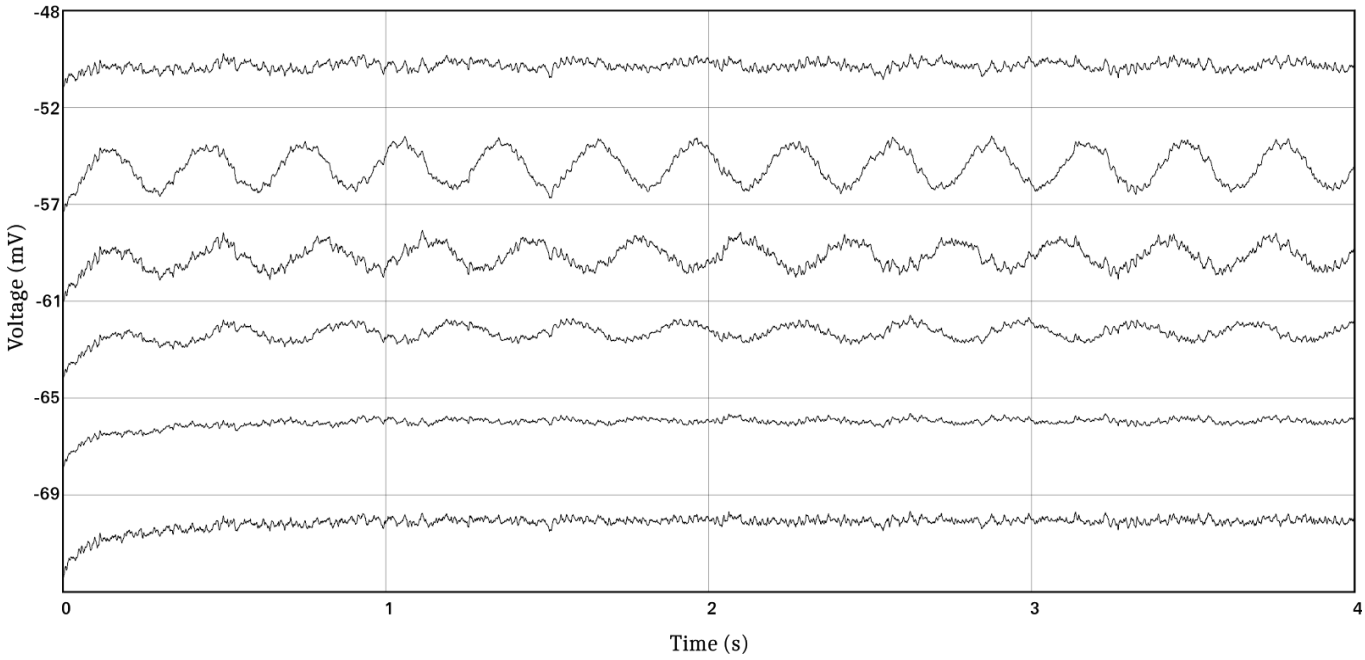

Fig 3: Sub-threshold Oscillations in Minimal Model of SC

The amplitude and frequency of the membrane potential oscillations varies as the depolarization input is changed as is seen in experimental data. (Dickson, et al., 2000) At 55.3 mV the membrane potential oscillations exhibit maximum amplitude and frequency ~3Hz.

initiating the downward phase of the oscillation. The slow component of I_h considered to affect oscillations while the fast component plays a key role in clustering of action potentials. The phase lag between the two currents thus is crucial for the generation of membrane potential oscillations.

On injecting a hyperpolarizing current step to the SC model, a “sag” in the membrane potential is observed, which is characteristic of hyperpolarization activated currents and in accordance with the physiological evidence.(Dickson, et al., 2000) (Fig 5)

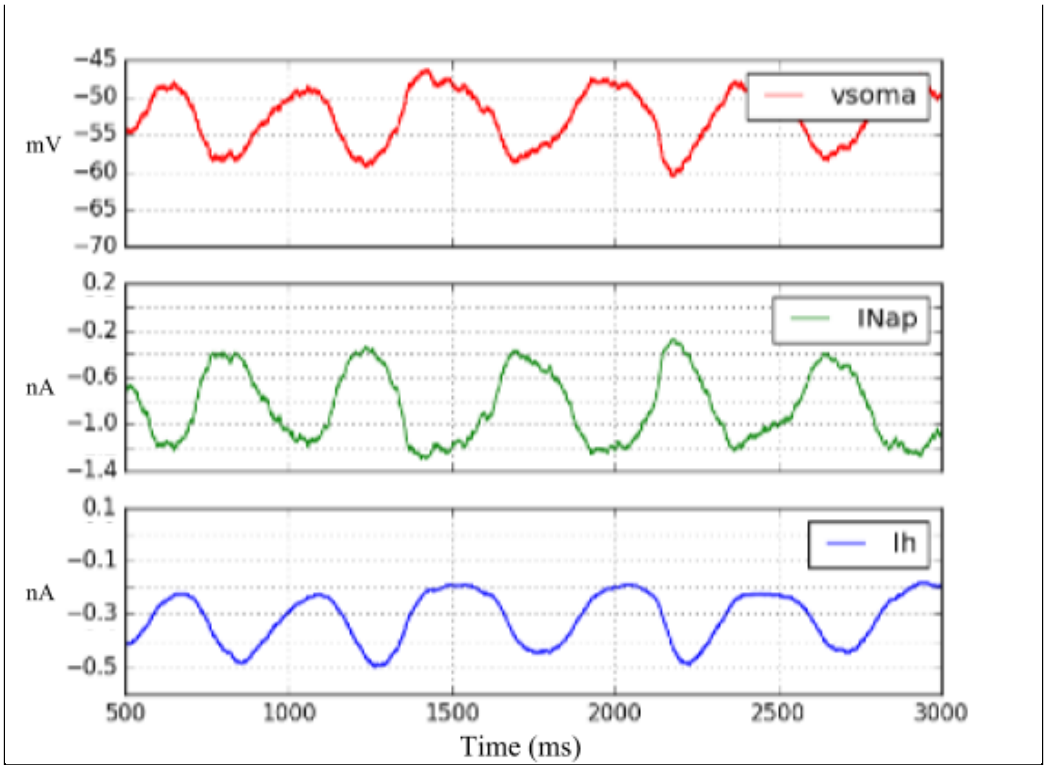

Fig 4: Phase relation between I_h and I_{NaP} The rise and fall of I_h correlates to the membrane potential oscillations and there is a phase lag between I_{NaP} and I_h.

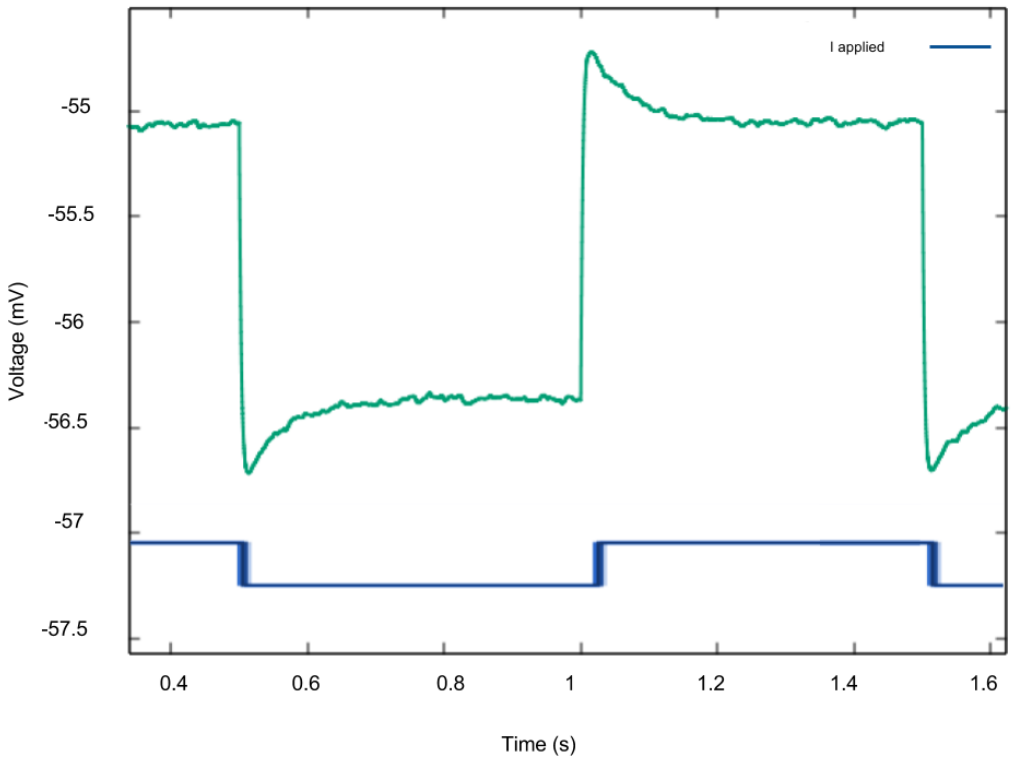

Fig 5: Membrane Potential “sag” during hyperpolarizing current step

The resting membrane potential of the minimal model ~ -55mV and the hyper-polarizing current step = -0.06nA.

The applied current step activates I_h progressively producing the “sag” as the membrane potential gradually increases while I_{NaP} remains constant. On release of the current, the membrane potential overshoots producing a repolarizing rebound known as medium afterhyperpolarization in current clamp recordings. Increasing the hyperpolarizing drive increased the rebound of the membrane potential after release but only to a certain extent without the spiking currents.

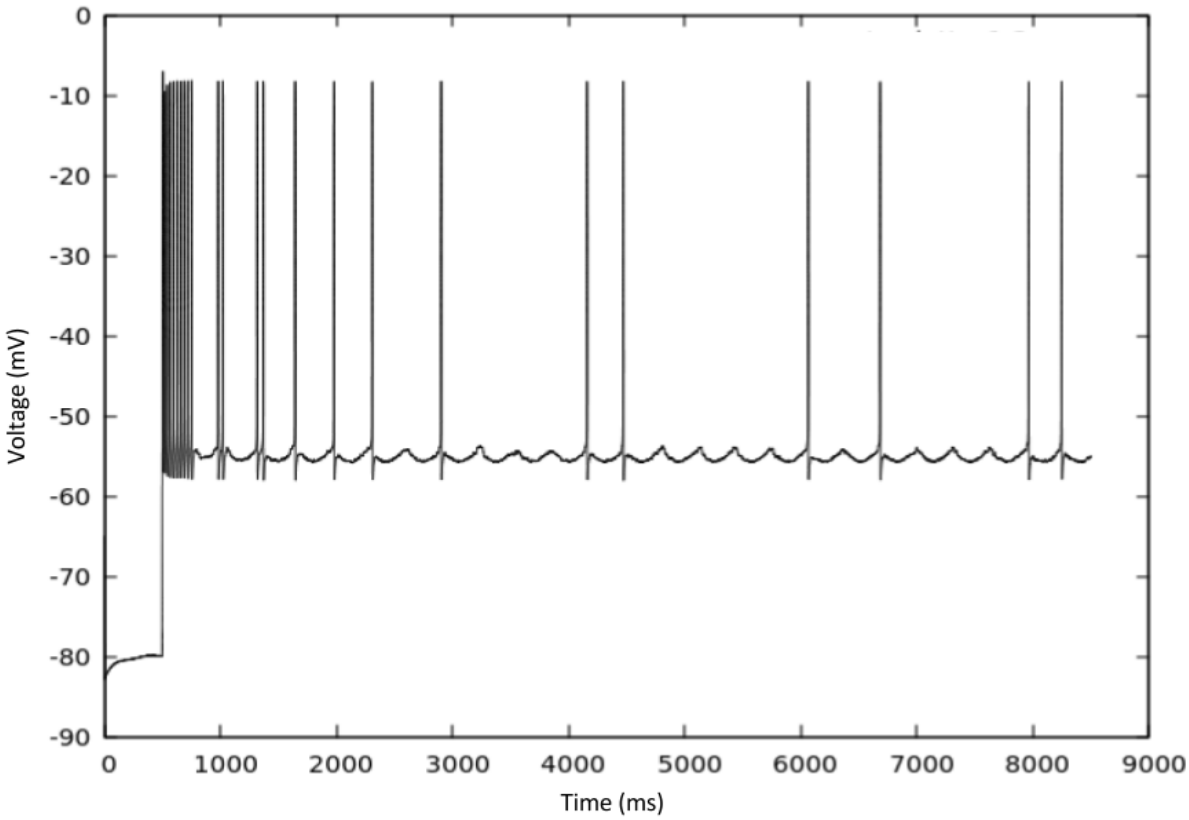

Fig 6: Mixed mode oscillations

The resting membrane potential of the detailed model ~ -56.2mV and the frequency of oscillations ~3Hz

I_h also plays a role in the clustering of action potentials and by introducing the rest of the currents in the detailed model, we observe mixed mode oscillations where the subthreshold oscillations are interspersed randomly with action potentials.(Fig 6)

.

On introducing depolarizing current steps of increasing in amplitude (Fig 7) we notice a gradual change from mixed-mode oscillations to formation of spike clusters, which continue to increase in density, to finally tonic firing. This increase in clustering corresponding to increase in current stimulation suggests that increase in hyperpolarization or inhibition would decrease spike clustering. This would indicate that inhibitory interneurons can modulate SC firing by the standard method inhibitory of hyperpolarization. (Rowland et al., 2016) Using the simple networks described in Fig 2 we can observe how varying inhibition by means of hyperpolarization can affect SC firing at a network level.

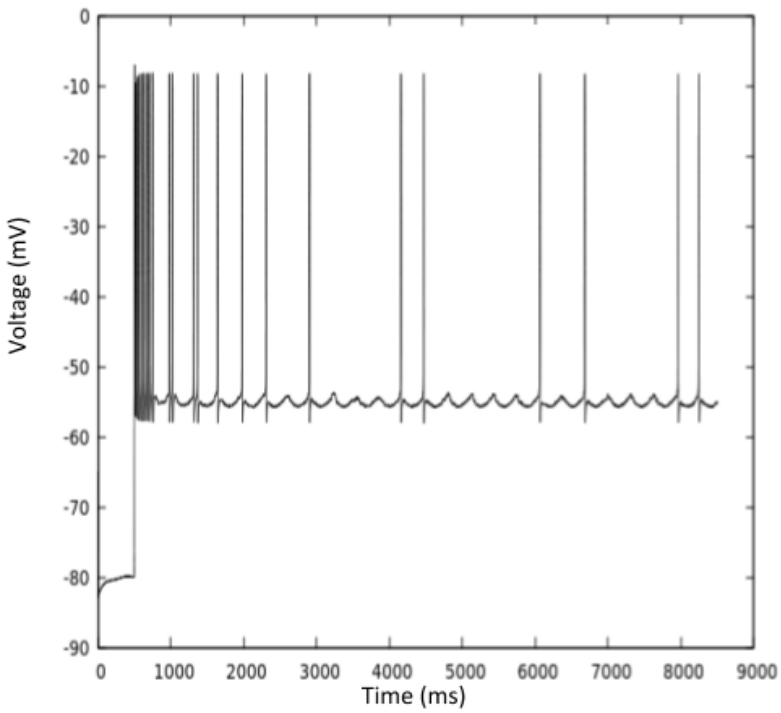

A

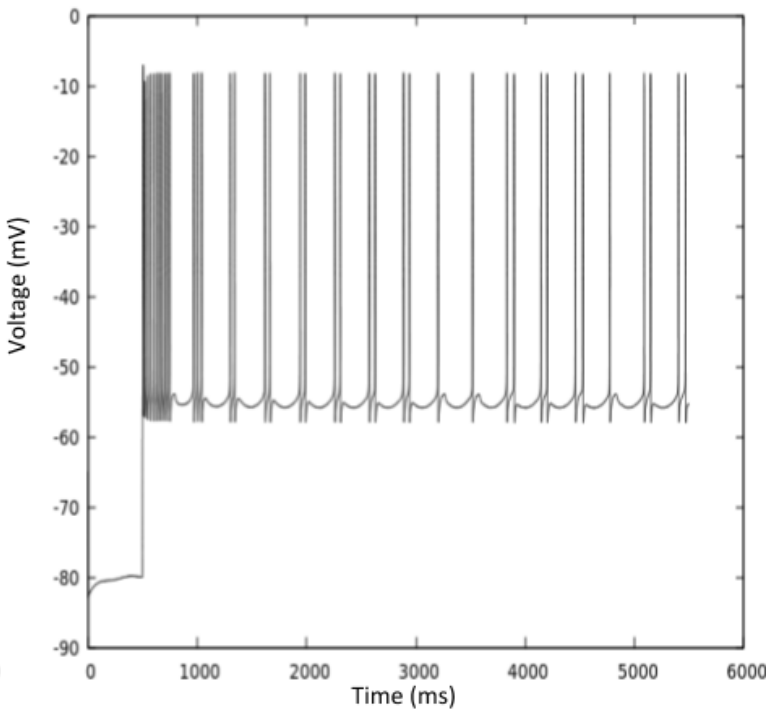

B

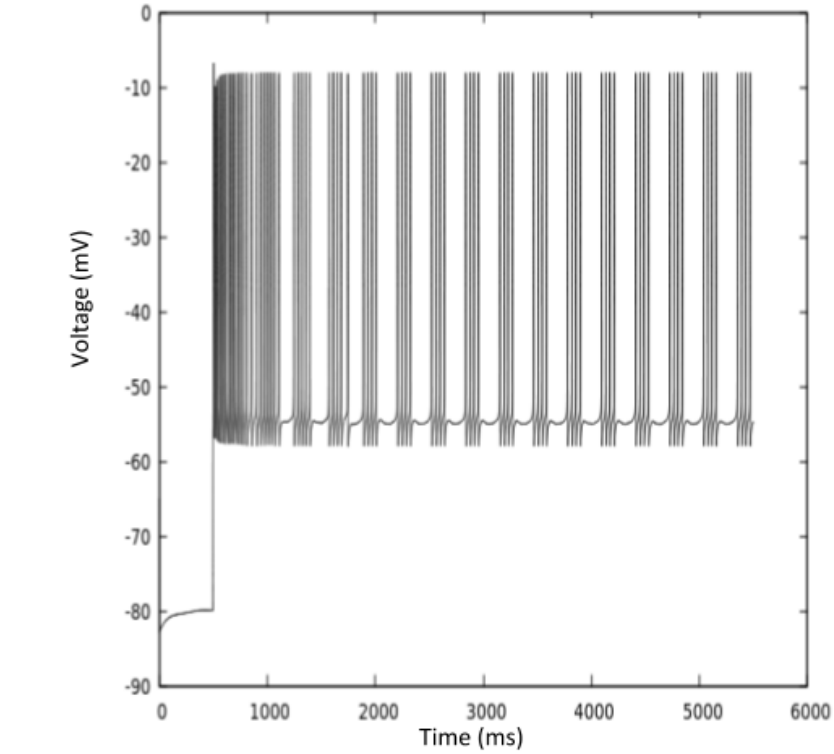
Voltage (mV)
0
-10
-20
-30
-40
-50
-60
-70
-80
-90
0
1000
2000
3000
4000
5000
6000
Time (ms)

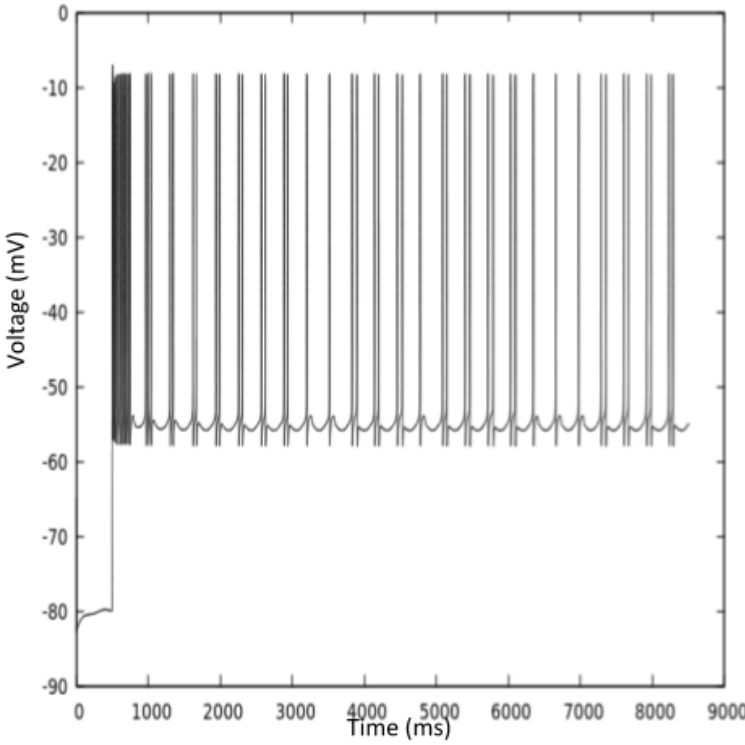
Voltage (mV)
0
-10
-20
-30
-40
-50
-60
-70
-80
-90
0
1000
2000
3000
4000
5000
6000
7000
8000
9000
Time (ms)

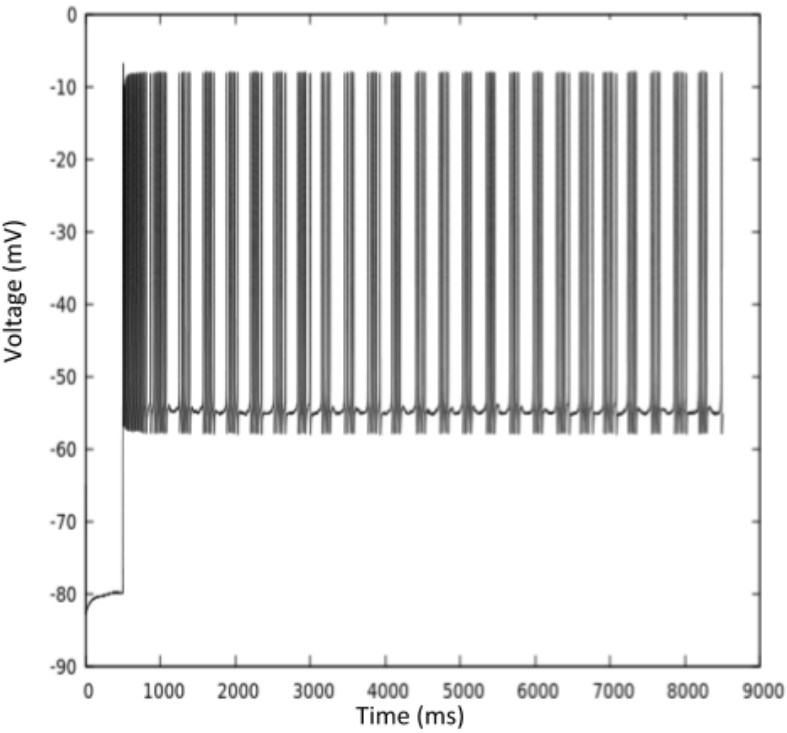
Voltage (mV)
0
-10
-20
-30
-40
-50
-60
-70
-80
-90
0
1000
2000
3000
4000
5000
6000
7000
8000
9000
Time (ms)

E

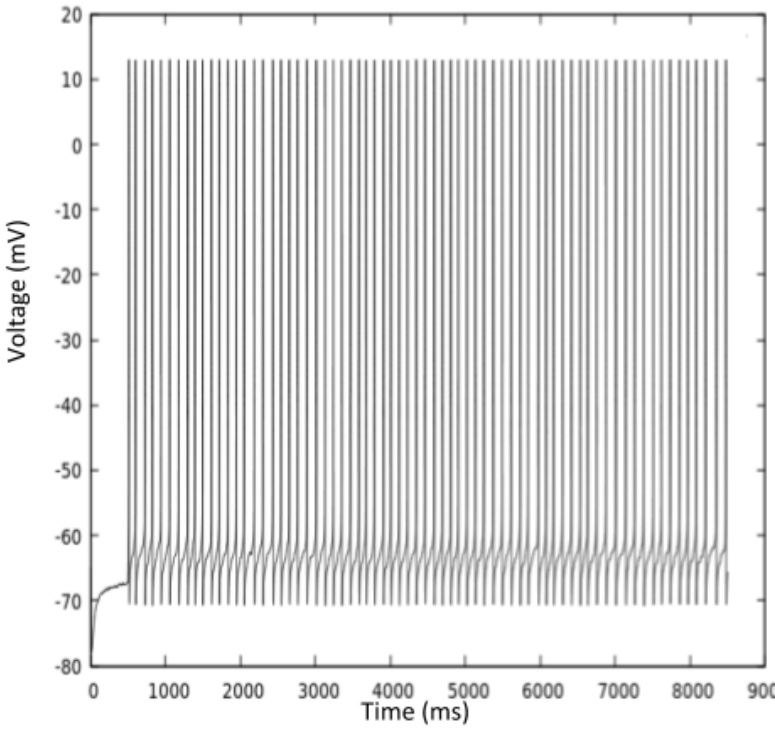
Voltage (mV)
20
10
0
-10
-20
-30
-40
-50
-60
-70
-80
0
1000
2000
3000
4000
5000
6000
7000
8000
9000
Time (ms)

F

Fig 7: Patterns of Spike Clustering

A depolarizing current step of 0.03nA was added in Fig A and increased by 0.01nA for each subsequent figure.

3.2 Effect of Inhibition on SC Networks

Fig 8: 2 SC and 1 IN Network

Alternate firing of two excitatory Stellate Cells without clustering out of phase.

In the network B, comprising of two SCs and one interneuron (IN), we do not see a clustering of action potentials of the two SCs out of phase as expected, but we do see a pattern of alternating spikes of the two neurons whose density decreases and inhibition is increased. (Fig 8) The lack of clustering could be attributed to the

absence of a after-hyperpolarizing potassium current from the simulations which is considered to play a role in clustering along with the slow component of I_h .

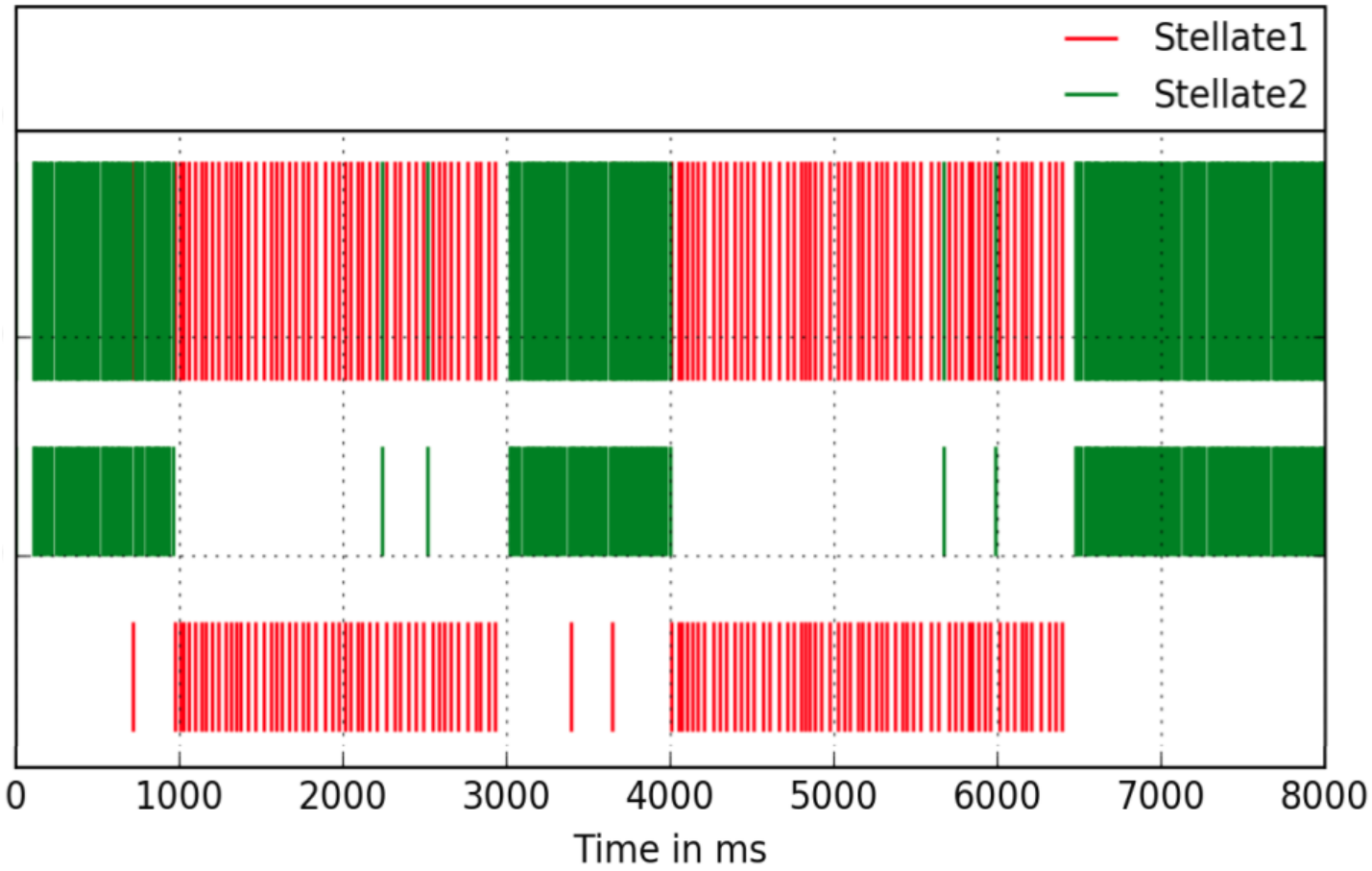

Fig 9: 2 SC and 2 IN Network

Alternate firing of two excitatory Stellate Cells clustering out of phase indicative of mechanism of firing fields.

In network C, comprising of two SCs and two INs, we observe a pattern of clustering of action potentials where the two excitatory neuron fire out of phase. (Fig 9)

From our model, we see that increase in inhibition causes an increase in the interburst interval i.e. the difference between two spike clusters of the same neuron. It also regulates the duration of the cluster of action potential spikes of the two stellate cells. In larger networks and more complex networks including multiple

excitatory and inhibitory neurons, the excitatory neurons form two groups which fire alternatively similar to what we observe in the 2 SC and 2 IN case mentioned above. By understanding how inhibition regulates the firing of SCs we can try to generate hexagonal firing fields by simulating much larger networks of our stellate cells and observing the effect of inhibition on patterns of these firing fields over time.

When an animal is introduced to a novel environment, its grid cell firing patterns have been shown to undergo changes. These distance between vertices of the grid expands initially, causing the grid patterns to expand in scale and grow irregular. Upon familiarization with the environment, these patterns revert to a smaller scale (Barry et al., 2012). These changes are independent of changes in environmental geometry and there is an inverse relationship between the scale of grid cell patterns and the theta band modulation of grid cell firing suggesting that these changes might be due to an endogenous effect. Using our detailed model of SCs, we can look at the changes in the intrinsic properties of SCs due to variation in inhibition and thus we can check whether inhibitory plasticity could be a potential mechanism behind the change in grid cell firing patterns in a novel environment and study how this would affect the properties of SCs.

We can further study the effect of spike timing dependent plasticity on our SC networks to potentially understand how the network of realistically modeled SCs and INs is regulated and its potential effect on grid cell firing fields. Understanding these mechanisms governing the cellular and network level properties of stellate cells can help provide insights into the factors governing grid cell firing fields and spatial representation.

4. References

1. Alonso, A, & Klink, R. (1993). Differential electroresponsiveness of stellate and pyramidal-like cells of medial entorhinal cortex layer II. *Journal of Neurophysiology*, *70*(1), 128–143.
2. Barry, C., Ginzberg, L.L., O'Keefe, J., and Burgess, N. (2012). Grid cell firing patterns signal environmental novelty by expansion. *Proc. Natl. Acad. Sci. U. S. A. 109*, 17687–17692.
3. Brun, V. H. (2002). Place cells and place recognition maintained by direct entorhinal[ndash]hippocampal circuitry . *Science* , *296* (2002), 2243–2246. http://doi.org/10.1126/science.1071089
4. Burgess, N., Barry, C., & O'Keefe, J. (2007). An Oscillatory Interference Model of Grid Cell Firing. *Hippocampus*, *17*(9), 801–812. http://doi.org/10.1002/hipo
5. Canto, C. B., & Witter, M. P. (2012). Cellular properties of principal neurons in the rat entorhinal cortex. II. The medial entorhinal cortex. *Hippocampus*, *22*(6), 1277–1299. http://doi.org/10.1002/hipo.20993
6. Dickson, C. T., Magistretti, J., Shalinsky, M. H., Fransén, E., Hasselmo, M. E., & Alonso, a. (2000). Properties and role of I(h) in the pacing of subthreshold oscillations in entorhinal cortex layer II neurons. *Journal of Neurophysiology*, *83*(5), 2562–2579.
7. Dickson, C. T., Magistretti, J., Shalinsky, M., Hamam, B., & Alonso, a. (2000). Oscillatory activity in entorhinal neurons and circuits. Mechanisms and function. *Annals of the New York Academy of Sciences*, *911*(514), 127–150. http://doi.org/10.1111/j.1749-6632.2000.tb06723.x
8. Eichenbaum, H., Dudchenko, P., Wood, E., Shapiro, M., & Tanila, H. (1999). The hippocampus, memory, and place cells: Is it spatial memory or a memory space? *Neuron*, *23*, 209–226. http://doi.org/10.1016/S0896-6273(00)80773-4
9. Etienne, A. S., & Jeffery, K. J. (2004). Path integration in mammals. *Hippocampus*, *14*(2), 180–192. http://doi.org/10.1002/hipo.10173
10. Fransén, E., Alonso, A. A., Dickson, C. T., Magistretti, J., & Hasselmo, M. E. (2004). Ionic mechanisms in the generation of subthreshold oscillations and action potential clustering in entorhinal layer II stellate neurons. *Hippocampus*, *14*(3), 368–384. http://doi.org/10.1002/hipo.10198

11. Fyhn, M., Molden, S., Witter, M. P., Moser, E. I., & Moser, M.-B. (2004). Spatial Representation in the Entorhinal Cortex. *Science*, *305*(5688).

12. Garden, D. L. F., Dodson, P. D., O'Donnell, C., White, M. D., & Nolan, M. F. (2008). Tuning of Synaptic Integration in the Medial Entorhinal Cortex to the Organization of Grid Cell Firing Fields. *Neuron*, *60*(5), 875–889. http://doi.org/10.1016/j.neuron.2008.10.044

13. Giocomo, L. M., Zilli, E. a, Fransén, E., & Hasselmo, M. E. (2007). Temporal frequency of subthreshold oscillations scales with entorhinal grid cell field spacing. *Science*, *315*(5819), 1719–22. http://doi.org/10.1126/science.1139207

14. Haas, J. S., Nowotny, T., & Abarbanel, H. D. I. (2006). Spike-timing-dependent plasticity of inhibitory synapses in the entorhinal cortex. *Journal of Neurophysiology*, *96*, 3305–3313. http://doi.org/10.1152/jn.00551.2006

15. Hafting, T., Fyhn, M., Molden, S., Moser, M., & Moser, E. I. (2005). Microstructure of a spatial map in the entorhinal cortex. *Nature*, *436*(7052), 801–806. http://doi.org/10.1038/nature03721

16. Hampson, R. E., Heyser, C. J., & Deadwyler, S. A. (1993). Hippocampal cell firing correlates of delayed-match-to-sample performance in the rat. *Behavioral Neuroscience*, *107*(5), 715–739. http://doi.org/10.1037/0735-7044.107.5.715

17. Hodgkin, A. L., & Huxley, A. F. (1990). A quantitative description of membrane current and its application to conduction and excitation in nerve. *Bulletin of Mathematical Biology*, *52*(1-2), 25–71. http://doi.org/10.1007/BF02459568

18. Huguenard, J. R., & McCormick, D. A. (1992). Simulation of the currents involved in rhythmic oscillations in thalamic relay neurons. *Journal of Neurophysiology*, *68*(4), 1373–1383.

19. Jones, R. S. G., & Bühl, E. H. (1993). Basket-like interneurones in layer II of the entorhinal cortex exhibit a powerful NMDA-mediated synaptic excitation. *Neuroscience Letters*, *149*(1), 35–39. http://doi.org/10.1016/0304-3940(93)90341-H

20. Klink, R., & Alonso, A. (1997). Morphological characteristics of layer II projection neurons in the rat medial entorhinal cortex. *Hippocampus*, *7*(5), 571–583. http://doi.org/10.1002/(SICI)1098-1063(1997)

21. Kropff, E., Carmichael, J. E., Moser, M.-B., & Moser, E. I. (2015). Speed cells in the medial entorhinal cortex. *Nature*, *523*, 419–424. http://doi.org/10.1038/nature14622

22. Leutgeb, S. (2005). Independent Codes for Spatial and Episodic Memory in Hippocampal Neuronal Ensembles. *Science*, *309*(5734), 619–623. http://doi.org/10.1126/science.1114037

23. Magistretti, J., & Alonso, A. (1999). Biophysical properties and slow voltage-dependent inactivation of a sustained sodium current in entorhinal cortex layer-II principal neurons: a whole-cell and single-channel study. *The Journal of General Physiology*, *114*(4), 491–509. http://doi.org/10.1085

24. Magistretti, J., Ragsdale, D. S., & Alonso, A. (1999). Direct demonstration of persistent Na+ channel activity in dendritic processes of mammalian cortical neurones. *The Journal of Physiology*, *521 Pt 3*, 629–36. http://doi.org/10.1111/j.1469-7793.1999.00629.x

25. McCormick, D. A., & Huguenard, J. R. (1992). A model of the electrophysiological properties of thalamocortical relay neurons. *Journal of Neurophysiology*, *68*(4), 1384–1400. http://doi.org/10.1073/pnas.0712231105

26. McNaughton, B. L., Battaglia, F. P., Jensen, O., & Moser, E. I. (2006). Path integration and the neural basis of the " cognitive map ." *Nature Neuroscience*, *7*(August), 663–678. http://doi.org/10.1038/nrn1932

27. Moser, E. I., Kropff, E., & Moser, M.-B. (2008). Place cells, grid cells, and the brain's spatial representation system. *Annual Review of Neuroscience*, *31*, 69–89. http://doi.org/10.1146/annurev.neuro.31.061307.090723

28. Nadel, L. (1991). The hippocampus and space revisited. *Hippocampus*, *1*(3), 221–229. http://doi.org/10.1002/hipo.450010302

29. O'Keefe, J. (1976). Place units in the hippocampus of the freely moving rat. *Experimental Neurology*, *51*(1), 78–109. http://doi.org/10.1016/0014-4886(76)90055-8

30. O'Keefe, J., & Conway, D. H. (1978). Brain Hippocampal Place Units in the Freely Moving Rat : Why They Fire Where They Fire. *Experimental Brain Research*, *31*(4), 573–590. http://doi.org/10.1007/BF00239813

31. O'Keefe, J., & Dostrovsky, J. (1971). The hippocampus as a spatial map. Preliminary evidence from unit activity in the freely-moving rat. *Brain Research*, *34*(1), 171–175. http://doi.org/10.1016/0006-8993(71)90358-1

32. Pastalkova, E., & Buzsaki, G. (2008). Internally Generated Cell Assembly Sequences in the Rat Hippocampus. *Science*, *321*(5894), 1322–1327. http://doi.org/10.1126/science.1159775.Internally

33. Pastoll, H., Ramsden, H. L., & Nolan, M. F. (2012). Intrinsic electrophysiological properties of entorhinal cortex stellate cells and their contribution to grid cell firing fields. *Frontiers in Neural Circuits*, *6*(April), 1–21. http://doi.org/10.3389/fncir.2012.00017

34. Quirk, G. J., Muller, R. U., & Kubie, J. L. (1990). The firing of hippocampal place cells in the dark depends on the rat's recent experience. *Journal of Neuroscience*, *10*(6), 2008–2017.

35. Rowland, D. C., Roudi, Y., Moser, M.-B., & Moser, E. I. (2016). Ten Years of Grid Cells. *Annual Review of Neuroscience*, *39*(1), annurev–neuro–070815–013824. http://doi.org/10.1146/annurev-neuro-070815-013824

36. Samsonovich, a, & McNaughton, B. L. (1997). Path integration and cognitive mapping in a continuous attractor neural network model. *The Journal of Neuroscience : The Official Journal of the Society for Neuroscience*, *17*(15), 5900–5920.

37. Sargolini, F., Fyhn, M., Hafting, T., McNaughton, B. L., Witter, M. P., Moser, M.-B., & Moser, E. I. (2006). Conjunctive Representation of Position, Direction, and Velocity in Entorhinal Cortex. *Science*, *312*(2006), 758–763. http://doi.org/10.1126/science.1099901

38. Schmidt-Hieber, C., Häusser, M., & Hausser, M. (2013). Cellular mechanisms of spatial navigation in the medial entorhinal cortex. *Nature Neuroscience*, *16*(3), 325–31. http://doi.org/10.1038/nn.3340

39. Sterratt, David, et al. (2011). *Principles of computational modelling in neuroscience*, *(Chapter 1)*. Cambridge University Press.

40. Tolman, E. C. (1948). Cognitive maps in rats and men. *Psychological Review*, *55*(4), 189–208. http://doi.org/10.1037/h0061626

41. Traub, R. D., Jefferys, J. G., Miles, R., Whittington, M. a, & Tóth, K. (1994). A branching dendritic model of a rodent CA3 pyramidal neurone. *The Journal of Physiology*, *481* , 79–95.

42. Traub, R. D., Wong, R. K., Miles, R., & Michelson, H. (1991). A model of a CA3 hippocampal pyramidal neuron incorporating voltage-clamp data on intrinsic conductances. *Journal of Neurophysiology*, *66*(2), 635–650.

43. White, J. a, Klink, R., Alonso, a, & Kay, a R. (1998). Noise from voltage-gated ion channels may influence neuronal dynamics in the entorhinal cortex. *Journal of Neurophysiology*, *80*(1), 262–269. http://doi.org/10.1038/342175a0

44. Wilson, M. A., & McNaughton, B. L. (1993). Dynamics of the Hippocampal Ensemble Code for Space Author (s): Matthew A . Wilson and Bruce L . McNaughton Published by : American Association for the Advancement of Science Stable URL http://www.jstor.org/stable/288186

45. Xiao-Jing Wang and György Buzsáki. (1996). Gamma Oscillation by Synaptic Inhibition in a Hippocampal Interneuronal Network Model. *The Journal of Neuroscience*, *16*(20), 6402–6413. http://doi.org/citeulike-article-id:134404

46. Zilli, E. a. (2012). Models of grid cell spatial firing published 2005-2011. *Frontiers in Neural Circuits* .http://doi.org/10.3389/fncir.2012.00016

5. Appendix

5.1 Conductances of currents in all compartments

The maximal conductances for all the ionic currents present the the detailed model of the stellate cell for each compartment are listed below.

Comp	Na	K_{dr}	K_c	Ca_L	h_f	h_s	NaP	K_{Leak}	ϕ
Soma	3.8	10.7	1340	0.1	0.112	0.0605	0.069	0.12	$61.34e^{12}$
IS	15	21.5	0	0	0	0	0	0.12	0
PD	3.8	10.7	0	0.1	0.112	0.0605	0.069	0.12	$97.37e^{12}$
MD	3.8	10.7	0	0.1	0.112	0.0605	0.069	0.12	$97.37e^{12}$
DD	1.9	5.4	0	0.1	0.112	0.0605	0.069	0.12	$21.91e^{12}$
PL	3.8	10.7	0	0.1	0.112	0.0605	0.069	0.12	$16.73e^{12}$
DL	1.9	5.4	0	0.1	0.112	0.0605	0.069	0.12	$3.76e^{12}$

IS – Initial Segment
PD, MD, DD – Proximal, Medial and Distal Primary Dendrite
PL, DL – Proximal and Distal Dendritic Lump

The units of all values are denoted in $mS/cm^{2.}$

The Ca^{2+} diffusion and buffering are modeled according to (Fransén et al., 2004; Huguenard & McCormick, 1992). ϕ represents the conversion factor of calcium from charge density to concentration present. While modeling the calcium dependent potassium current, the minimal $[Ca^{2+}]$ is set to $5*10^{-6}$ and the diffusion rate is 0.5ms.

5.2 Parameters of currents of Interneurons

The activation and inactivation parameters for the currents in the interneuron model are as follows.

Na Current: (E_{rev} = + 55mV) $g_{Na} = 52mS/cm^2$

Activation: (m)

$$\alpha_m(V) = \frac{0.1\ (V+35)}{1\ -\ exp(-\frac{(V+35)}{10})}$$

$$\beta_m(V)\frac{-4\ exp(V+60)}{18}$$

$$\text{Gate exponent} = 3$$

Inactivation: (h)

$$\alpha_h(V)\frac{-0.07\ exp(V+58)}{20}$$

$$\beta_h(V) = \frac{1}{1+(exp(-0.1\ *\ (V+28))}$$

$$\text{Gate exponent} = 1$$

Kdr Current: (E_{rev} = - 90mV) $g_K = 9mS/cm^2$

Activation: (n)

$$\alpha_n(V) = \frac{0.01\ (34+V)}{1\ -\ exp(-0.1\ *\ (V+34)}$$

$$\beta_n(V) = 0.125\ *\ exp - \frac{(V+44)}{80}$$

$$\text{Gate exponent} = 4$$